

MoA: MIXTURE OF SPARSE ATTENTION FOR AUTOMATIC LARGE LANGUAGE MODEL COMPRESSION

Tianyu Fu^{1,2,*}, Haofeng Huang^{1,2,*}, Xuefei Ning^{1,*}, Genghan Zhang³, Boju Chen¹,
Tianqi Wu^{1,2}, Hongyi Wang^{1,2}, Zixiao Huang^{1,2}, Shiyao Li^{1,2},
Shengen Yan^{1,2}, Guohao Dai^{2,4}, Huazhong Yang¹, Yu Wang¹

¹Tsinghua University ²Infinigence-AI ³Stanford University ⁴Shanghai Jiao Tong University

ABSTRACT

Sparse attention can effectively mitigate the significant memory and throughput demands of Large Language Models (LLMs) in long contexts. Existing methods typically employ a uniform sparse attention mask, applying the same sparse pattern across different attention heads and input lengths. However, this uniform approach fails to capture the diverse attention patterns inherent in LLMs, ignoring their distinct accuracy-latency trade-offs. To address this challenge, we propose the Mixture of Attention (MoA), which automatically tailors distinct sparse attention configurations to different heads and layers. MoA constructs and navigates a search space of various attention patterns and their scaling rules relative to input sequence lengths. It profiles the model, evaluates potential configurations, and pinpoints the optimal sparse attention compression plan. MoA adapts to varying input sizes, revealing that some attention heads expand their focus to accommodate longer sequences, while other heads consistently concentrate on fixed-length local contexts. Experiments show that MoA increases the effective context length by $3.9\times$ with the same average attention span, boosting retrieval accuracy by $1.5 - 7.1\times$ over the uniform-attention baseline across Vicuna- $\{7B, 13B\}$, and Llama3- $\{8B, 70B\}$ models. Moreover, MoA narrows the capability gaps between sparse and dense models, reducing the maximum relative performance drop from $9\% - 36\%$ to within 5% across two long-context understanding benchmarks. MoA achieves a $1.2 - 1.4\times$ GPU memory reduction, boosting decode throughput by $6.6 - 8.2\times$ and $1.7 - 1.9\times$ compared to FlashAttention2 and vLLM, with minimal impact on performance. Our code is available at <https://github.com/thu-nics/MoA>.

1 INTRODUCTION

Large Language Models (LLMs) exhibit remarkable versatility across numerous applications (Brown et al., 2020; Tay et al., 2022; Wan et al., 2023). Central to LLM is the attention mechanism (Vaswani et al., 2017), which computes interactions among tokens within a certain span, thereby enabling context understanding. Scaling input length is crucial for enhancing LLM capabilities (Chen et al., 2023; Tworowski et al., 2023), including fact retrieval, summarization, few-shot learning, question answering and so on (Bai et al., 2023; Yuan et al., 2024). However, the ever-growing attention computation and Key-Value Cache (KV-Cache) pose significant efficiency challenges (Sheng et al., 2023; Xiao et al., 2024c; Han et al., 2023; Kwon et al., 2023).

Previous work proposes sparse attention methods to address the efficiency challenges of long contexts in generative LLMs. These methods typically employ a uniform, fixed-span sliding window mask across all heads and input lengths, limiting attention to local contexts only (Xiao et al., 2024c; Han et al., 2023). This approach allows the LLM to take long inputs with a fixed attention span, keeping bounded attention computation and KV caching overhead. Following previous works (Chen et al., 2023; Tworowski et al., 2023), we quantify the effective context length as the maximum input length where content retrieval accuracy exceeds a 90% threshold. In principle, fixed-span

*Equal contribution. Genghan Zhang made contributions while at Tsinghua University
Corresponding author: Xuefei Ning (foxdoraame@gmail.com)

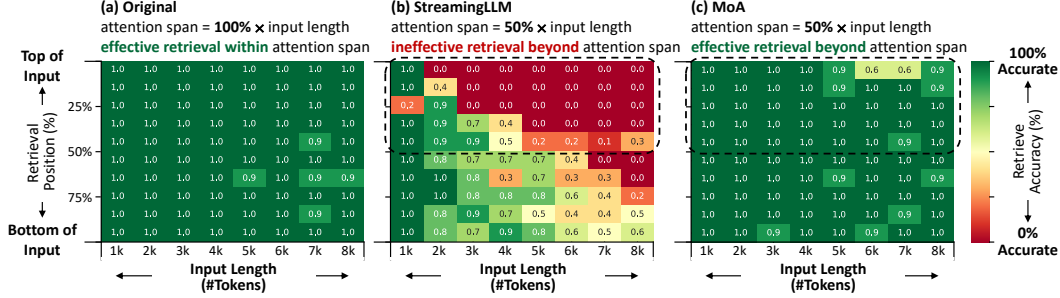


Figure 1: Retrieval accuracy of the Vicuna-7B model using different attention methods across varying input lengths and retrieval positions on the LongEval benchmark (Li et al., 2023). This retrieval benchmark takes massive key-value pairs as inputs and tests the accuracy to retrieve values based on given keys from diverse positions. (a) Original model with a full attention span; (b) StreamingLLM with half the attention span, showing reduced effectiveness beyond the span; (c) MoA with half the attention span, maintaining effectiveness beyond the span.

local attention can gradually aggregate global information through multiple model layers, yielding a longer effective context length than each attention span (Feng et al., 2022; Zaheer et al., 2020). Nonetheless, we reveal that uniform masks, like StreamingLLM (Xiao et al., 2024c), hardly extend effective context length beyond the span, as shown in Figure 6. Figure 1(b) further illustrates such limitation: with a 50% attention span mask, StreamingLLM fails to accurately retrieve content from the earlier half of the input and performs even worse at longer input lengths. Figure 2 reveals one possible explanation for the problem: while some attention heads focus on local contexts, others encompass the broad span of the entire input sequence. Consequently, the uniform approach fails to achieve a long effective context length as it limits the attention span of the global-context heads, while excessively allocates compute and memory budget for local-context heads. Additionally, as the input length increases, some attention heads need a faster increase in attention span than others to avoid serious performance degradation, as shown in Table 1. Unfortunately, the uniform approaches do not include heterogeneous rules to scale the attention spans differently for various heads. Besides, existing model compression methods (Men et al., 2024; Lin et al., 2023; Xiao et al., 2024b; Li et al., 2024a; Kim et al., 2023; Li et al., 2024b) use *general language modeling corpora* to decide the compression plan, which cannot accurately profile the influence of compression on *long-context tasks*.

In this work, we propose Mixture of Attention (MoA), a training-free sparse attention method. As illustrated in Figure 3, MoA constructs the search space of heterogeneous elastic rules of attention spans. For automatic LLM compression, MoA first utilizes gradient-based profiling to inspect the influences of each attention position on the prediction loss. Based on the profiling results, MoA tailors heterogeneous sparse attention configurations for each model layer and attention head. During profiling, MoA employs a calibration dataset with long-range dependencies and uses the original dense model’s response instead of the human-written response as the reference to calculate the loss. This ensures an accurate profiling of the attention influences to facilitate better compression results. Our contributions are summarized as follows.

- **Heterogeneous Elastic Rules.** We propose heterogeneous elastic rules for masks of each attention head. We formulate MoA compression search space to include a diverse range of elastic rules that tailor the local attention span relative to the input length for each attention head. The heterogeneous elastic rules improve the fact retrieval accuracy of MoA from 25% to 98% compared with masks with uniform span and scaling function for each head.
- **Calibration Dataset Construction** We emphasize the importance of data engineering in LLM compression. Our findings demonstrate that, instead of relying on general language modeling datasets and human responses, using datasets with long-range dependencies and referencing the original LLM’s responses is essential for accurately profiling the effects of compression.
- **Automatic Optimization.** We propose an automatic pipeline to find the optimal compression plan encompassing heterogeneous elastic rules for various attention heads. This pipeline can

efficiently find the optimal plan within several hours, for example, two hours for compressing Vicuna-13B.

Experiments show that MoA achieves $6.6 - 8.2\times$ throughput improvements over FlashAttention2, $1.7 - 1.9\times$ over vLLM framework on 7B and 13B dense LLMs at a 50% density (the average of KV-Cache length / input length), with only a 1% average relative degradation in retrieval accuracy. In Section 6.4, we show that this significant throughput improvements of MoA over FlashAttention2 can be attributed to four factors: (1) the static size of the KV-cache, (2) reduced attention computations, (3) increased batch size enabled by reduced memory usage, and (4) a specialized kernel implementation. Additionally, MoA achieves over 90% retrieval accuracy with just 25% average density, far surpassing sparse attention baselines that need a density of 75% to 100% for similar performance. On long-context understanding benchmarks, MoA performs comparably to dense models, with a maximum relative performance drop of less than 5%, which is about one-sixth of that observed with the uniform sparse attention baseline. Our code is available at <https://github.com/thu-nics/MoA>.

2 PRELIMINARY AND RELATED WORK

2.1 ATTENTION MECHANISM

The Multi-Head Self Attention (MHA) mechanism (Vaswani et al., 2017) is crucial to the functionality of LLMs. It starts with an input sequence transformed into query (Q), key (K), and value (V) matrices through linear projections. These matrices, combined with the cached K and V (KV-Cache) from previous sequences, compute the attention matrix (A). This calculation is modified by a causal mask (M) to ensure autoregressive properties, resulting in the output (O), as depicted in Equation 1:

$$\mathbf{S} = \mathbf{QK}^T, \quad \mathbf{A} = \text{softmax}(\mathbf{S} + \mathbf{M}), \quad \mathbf{O} = \mathbf{AV} \quad (1)$$

Autoregressive inference in LLMs involves two stages: prefill and decode. During prefill, the model processes the entire input sequence to generate the initial response token. In the subsequent decode stage, it uses the newly generated token and previously cached K and V matrices to produce subsequent tokens until the generation concludes. Although effective, this iterative process increases memory and computation demands due to the expanding KV-Cache.

2.2 EFFICIENT ATTENTION

Efficient methods are proposed to mitigate the computation and memory costs associated with attention. One branch of work uses dynamic sparse attention masks to adaptively skip attention computations during prefill stage (Pagliardini et al., 2023; Qu et al., 2022; Roy et al., 2021; Wang et al., 2021; Lu et al., 2021; Kitaev et al., 2020) or drop KV-Cache during decode stage (Anagnostidis et al., 2023; Zhang et al., 2023; Ge et al., 2023; Sheng et al., 2023; Liu et al., 2023a) based on the input sequences. However, due to the complex control and computation flow, dynamic prefill often requires specific hardware to achieve substantial wall-time speedup (Qu et al., 2022; Wang et al., 2021; Lu et al., 2021; Ham et al., 2021; 2020). Additionally, dynamic KV-Cache pruning in the decode stage may require extensive retraining (Anagnostidis et al., 2023), additional accumulated attention score computation (Sheng et al., 2023; Zhang et al., 2023; Liu et al., 2023a; Ge et al., 2023), or extensive memory swap for KV-Cache retrieval (Tang et al., 2024; Xiao et al., 2024a).

Another branch of work uses static sparse attention, where predefined masks are applied consistently across all processed sentences. Thanks to the fixed computation flow, static sparse attention is generally more efficient and GPU-friendly. For language understanding models such as BERT (Devlin et al., 2018), various masks are used (Zaheer et al., 2020; Beltagy et al., 2020; Child et al., 2019; Zhou et al., 2024; Xiao et al., 2024c; Han et al., 2023). But for generative LLMs, the predominant method is the fixed-span sliding window mask with global attention on a few initial tokens (Xiao et al., 2024c; Han et al., 2023). With the local attention pattern, the KV-Cache beyond the current attention span can be dropped, saving much memory for long sequence scenarios. However, the uniform static masks across different attention heads and input lengths are model- and data-agnostic, which can compromise LLMs’ effective context length and lead to suboptimal performance in long sequence scenarios. Our method falls within this category, benefiting from the efficiency and training-free advantages, while addressing the performance limitations encountered by previous methods.

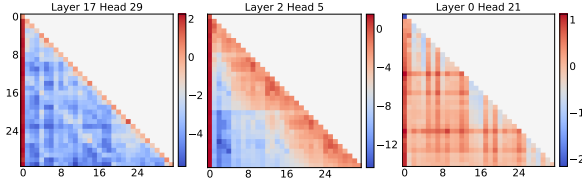


Figure 2: Examples of attention matrices from different attention heads of the Vicuna-7B model. Each attention matrix is averaged over 256 data items from the LongEval dataset.

Layers	Window/Input Len.		
	2k/4k	2k/8k	4k/8k
6, 7, 8	0.83	0.29	0.61
9, 10, 11	0.99	0.81	0.96
17, 18, 19	0.97	0.94	0.97

Table 1: Retrieval accuracy of Vicuna-7B with sliding-window sparse attention across various model layers, window spans, and input lengths.

In addition to sparse attention, alternative mechanisms have been proposed to replace traditional attention for long-sequence modeling (Gu & Dao, 2023; Peng et al., 2023; Sun et al., 2023; Poli et al., 2023; Li et al., 2022; Kacham et al., 2023; Peng et al., 2021; Choromanski et al., 2020; Wang et al., 2020). However, these new mechanisms often require different weights compared to vanilla transformers, imposing significant re-training overhead for LLMs.

Previous works also propose LLM acceleration frameworks (Gugger et al., 2022; Aminabadi et al., 2022; Sheng et al., 2023; Kwon et al., 2023), as well as kernel-level optimizations (Dao et al., 2022; Dao, 2023; Shah et al., 2024). These kernel and system optimizations are orthogonal to our work and can be integrated to further enhance efficiency.

3 MIXTURE OF ATTENTION (MOA)

We first illustrate the heterogeneity of the attention patterns in pre-trained LLMs in Section 3.1. Based on this insight, we define the search space for our Mixture-of-Attention (MoA) method in Section 3.2.

3.1 MIXTURE OF ATTENTION PATTERNS AND ELASTIC RULES

Heterogeneous Attention Patterns. Different attention heads in LLMs exhibit heterogeneous attention patterns, as shown in Figure 2. For example, the first head primarily focuses on local contexts with a narrow-span sliding window, while the third head covers nearly the entire input, indicating global attention. The attention spans of different heads mostly remain constant across various tasks and datasets, as shown in Appendix D.1. Table 1 demonstrates that applying the same sliding-window sparse attention mask across model layers can lead to a 65% variance in retrieval accuracies. It conforms to the multi-head self-attention design principle of capturing varied information (Vaswani et al., 2017), as well as the findings from concurrent research that identifies specific attention heads for global text retrieval (Wu et al., 2024).

Heterogeneous Elastic Rules. In addition to heterogeneity at a certain length, different attention heads also exhibit varying elastic behaviors as the input length changes. Figure 2 illustrates this variability: for shorter inputs (the upper left part of the attention matrix), the second and third heads initially show global attention. However, as input length increases, the second head remains the medium-span local focus, while the third head continues to expand as global attention. Table 1 further evidences the diverse elastic rules. For example, at 4k input length, a 2k sliding-window sparse attention mask on layers 9 to 11 yields better retrieval accuracy than on layers 17 to 19. However, the opposite is true for an 8k input length. This data supports the visual observations from Figure 2, highlighting that attention patterns respond to input length scaling differently. Leveraging these insights, MoA encompasses heterogeneous elastic rules as the search space.

3.2 HETEROGENEOUS ELASTIC RULE SEARCH SPACE

In designing the search space for the MoA mask, we consider the inherently heterogeneous and elastic nature of LLM attention patterns. As shown in Figure 3(a), we adopt a hardware-friendly sliding-window mask as our base sparse attention mask (Beltagy et al., 2020). Following previous work (Xiao et al., 2024c; Han et al., 2023), the initial few tokens (64 tokens for MoA) are not masked. The attention span equals the sliding-window-span plus the number of initial unmasked tokens. We

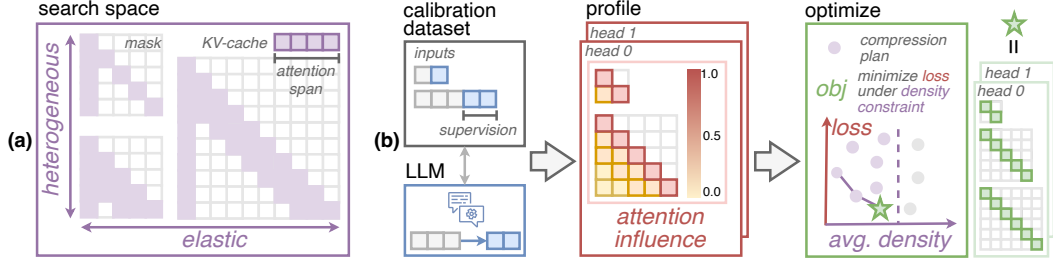


Figure 3: Overview of the MoA. (a) The sparse attention search space includes heterogeneous elastic rules of the attention span on sliding-window masks. (b) The automatic compression pipeline begins with a calibration dataset, which includes long-dependency contexts and supervision texts generated by the original dense LLM. MoA profiles each attention value’s impact on model predictions within this dataset, revealing accuracy losses for different candidate elastic rules across various input lengths. The final optimization step selects elastic rules for each attention head to minimize the total prediction loss while adhering to specified density constraints.

define the attention span S of head h at input length N using a straightforward linear function:

$$S_h = \alpha_h + \beta_h \cdot N, \quad (2)$$

where α_h and β_h are hyperparameters that control the base span and its expansion rate with input length of a specific attention head.

The α and β hyperparameters of each attention head can be chosen from multiple discrete options. For LLMs with many layers, the MoA search space can become quite large. For example, for a 7B model consisting of 32 attention heads and 32 layers, with 6 and 9 different α and β options for each head, the potential search space expands to 54^{1024} configurations. Thus, we design the automatic pipeline to efficiently pinpoint the optimal α s and β s for any LLM.

4 AUTOMATIC PIPELINE FOR MOA COMPRESSION

This section outlines the MoA automatic compression pipeline as shown in Figure 3(b). Starting with a trained LLM and a calibration dataset, MoA first **profiles** the influence of each attention value on the model’s prediction loss for various input sequences from the calibration dataset. The masked sum of the influences represents the accuracy loss associated with each mask at different input lengths, showing the accuracy loss each candidate elastic rule could cause at that length. Then, MoA **optimizes** the compression plan by selecting the optimal elastic rule for each head, which minimizes the accuracy loss across various lengths while adhering to specified density constraints. The following sections provide detailed discussions of each step in this pipeline.

4.1 ATTENTION INFLUENCE PROFILING

In the profile step, MoA quantifies the impact of individual attention values on the final prediction loss of a pre-trained LLM. It informs the subsequent step about the influence of masking each attention value, revealing the accuracy trade-offs of the candidate elastic rules for each attention head.

The influence of each attention value is derived from the attention matrix \mathbf{A} and its gradient $\partial L / \partial \mathbf{A}$, computed over a calibration dataset. When applying sparse attention masks, we approximate the change in the model’s prediction loss, ΔL , using a first-order Taylor expansion based on variations in the attention matrices \mathbf{A} : $\Delta L = \sum_h \sum_i \sum_j \partial L / \partial A_{h,i,j} \cdot \Delta A_{h,i,j}$. Here, h indexes the attention heads across all layers, and i, j are the row and column indices within each attention matrix \mathbf{A}_h .

We define the *attention influence* matrix, $E_{h,i,j}$, as the estimated change in loss, ΔL , if the attention value $A_{h,i,j}$ is masked (i.e., set to zero). As shown in Equation 3, this measure considers both the direct and indirect effects of the mask. For notation simplicity, we omit the head index h here. Initially, masking directly reduces the attention value to zero, represented by $\Delta A_{i,j|j} = -A_{i,j}$. Additionally, the softmax function in attention normalizes the sum of each row in the attention matrix to one. Thus, setting one attention value at column j to zero causes an increase in the other attention

values, $\Delta A_{i,n|j}$, $n \neq j$, within the same row. These two effects are integrated into the following formulation, whose derivation is provided in Appendix D.2:

$$E_{i,j} = \sum_n \frac{\partial L}{\partial A_{i,n}} \cdot \Delta A_{i,n|j} = \frac{\partial L}{\partial A_{i,j}} \cdot (-A_{i,j}) + \sum_{n \neq j} \frac{\partial L}{\partial A_{i,n}} \cdot A_{i,n} \cdot \frac{A_{i,j}}{1 - A_{i,j}} \quad (3)$$

In practice, we use backpropagation on a calibration dataset to calculate the average attention influence \bar{E}_h of each head across data items. The average attention influence is calculated respectively for different input lengths. The gradient $\partial L / \partial \mathbf{A}_h$ is computed using chain derivative in deep learning frameworks like PyTorch (Paszke et al., 2019). The detailed calibration dataset setup is discussed in Section 5.

With the average attention influence of each head, MoA can calculate the accuracy loss of applying a candidate elastic rule at a specific input length. The loss is calculated with the sum of masked average attention influence according to the rule. We denote \mathbf{M}_{r_h} as the binary mask at head h that corresponds to rule r , with masked positions marked as 1 and others as 0. We formalize accuracy loss ΔL as follows:

$$\Delta L = \sum_h \Delta L_{h,r_h} = \sum_h \sum_i \sum_j M_{r_h,i,j} \cdot \bar{E}_{h,i,j}. \quad (4)$$

After the profile stage, MoA acquires the unique accuracy-density trade-offs of elastic rules. It informs the allocation of denser masks to more sensitive heads and lighter masks to less sensitive ones. Profiling at different input lengths enables the identification of the most effective elastic rules, even for unseen lengths.

4.2 AUTOMATIC OPTIMIZATION

MoA automatically selects the optimal elastic rule for each attention head to minimize accuracy losses across various sequence lengths under density budgets. Based on the profiling results, MoA first identifies Pareto front compression plans where any improvement in accuracy loss at one profile length would worsen another. To ensure the best generalization to lengths beyond those profiled, MoA then selects the plan that yields the minimum loss at an unseen length among the Pareto front solutions as the final plan.

Specifically, we utilize multi-objective optimization to search for a set of Pareto optimal compression plans across the profiled lengths. The objective for each length is to minimize the total accuracy loss while conforming to any user-defined density constraints. The objective is formulated as follows:

$$\arg \min_{r_h \in \mathbb{R}} \Delta L^{(N_i)}, N_i \in \mathbb{N}_{\text{profile}} \quad \text{s. t.} \quad \frac{1}{H} \sum_{h=1}^H d_{r_h}^{(N_i)} \leq d_{\text{constr}}^{(N_i)}, \forall N_i \in \mathbb{N}_{\text{constr}}. \quad (5)$$

Here, superscript (N) denotes values at different lengths; $\mathbb{N}_{\text{profile}}$ and $\mathbb{N}_{\text{constr}}$ denote the sets of lengths for profiling and those subject to density constraints, respectively; \mathbb{R} denotes the set of candidate rules; $\Delta L^{(N_i)}$ denotes the accuracy loss due to compression; $d_{r_h}^{(N_i)}$ denotes the density of rule r_h at head h ; $d_{\text{constr}}^{(N_i)}$ denotes the average density constraint; H denotes the total number of attention heads.

Such formulation corresponds to the classic multi-objective mixed-integer-planning problem, which can be effectively solved within minutes using existing linear solvers, like Gurobi (Gurobi Optimization, LLC, 2023). The detailed problem formulation and solving strategies are discussed in Appendix D.3.

Among the Pareto optimal compression plans, we select the one with the minimum loss at the unseen validation length as the optimal solution. This approach allows us to avoid profiling at every possible length while increasing the likelihood that the plan will generalize effectively to unseen lengths.

Thanks to this automatic pipeline, we efficiently get the elastic rules tailored for each attention head. With the pipeline, MoA minimizes the accuracy loss caused by attention sparsification, while conforming to user-defined density constraints.

5 DATASET AND SUPERVISION

In this section, we highlight the overlooked importance of calibration dataset design and its supervision objective in LLM compression. Calibration datasets are essential for sensitivity analysis across various

Table 2: Calibration dataset design choices: dataset content, supervision, and response reference. Calibration dataset with long dependency and model alignment improves MoA performance on retrieval accuracy and perplexity. All tests are done at 25% average density at 8k input length.

Dataset	Supervision	Reference	Long Dep.	Align Model	Retrieval Acc. \uparrow	PPL \downarrow
RedPajama	Context	-	\times	\times	0.25	4.95
MultiNews	Context & Summary	Human	\times/\checkmark	\times	0.27	4.62
MultiNews	Summary	Human	\checkmark	\times	0.87	3.97
MultiNews	Summary	Model	\checkmark	\checkmark	0.95	3.96

compression techniques, including weight pruning (Men et al., 2024; Lee et al., 2024; Liu et al., 2023b) and quantization (Lin et al., 2023; Xiao et al., 2024b; Li et al., 2024a; Kim et al., 2023). In this work, MoA profiles the attention influence on the calibration dataset, which is crucial for subsequent automatic optimization.

Current Approach. General language modeling datasets, such as human-written text corpus RedPajama (Computer, 2023), are commonly used as the calibration dataset. These datasets, supervised by next-token-prediction on the entire corpus, primarily capture attention patterns coherent with immediately preceding tokens. However, they lack long context dependencies, failing to address the global attention crucial for tasks like long-range retrieval.

Moreover, a notable misalignment exists between the model response and the human-written supervision. Consequently, it leads to inaccuracies when using human responses to compute attention values and gradients during profiling. For example, given the same question, a human might answer ‘Blue’, while the model could generate ‘The blue color’. Using the human answer for supervision, attention influence is inaccurately quantified based on probability shift for predicting ‘Blue’; this diverges from the objective of maintaining crucial attention for the original model prediction, ‘The’. These inconsistencies arise from various factors, including mismatched positions, tones, and synonyms.

MoA’s Approach. MoA enhances the calibration dataset by integrating *long-range dependencies* and *model alignment*. Specifically, we utilize the long-contextual MultiNews dataset (Fabbri et al., 2019), which includes summaries heavily dependent on long-range content. The summaries are generated by the original dense model and serve as supervision. Compared to current approaches that adopt human responses as the reference to calculate the loss, using the responses generated by the original model as the supervision can facilitate accurate influence profiling, thus benefiting the compression results.

Approach Comparison. We evaluate our design’s effectiveness by varying dataset choices, supervision types, and summary references, while standardizing data item count and length to 50 and 8k words, respectively. Additional setups and evaluations are in Appendices A and B.3.1.

We show the importance of long-range dependencies by comparing the MoA compression plan generated with different datasets and supervisory methods. In Table 2, RedPajama (Computer, 2023) represents the general language modeling dataset, while MultiNews (Fabbri et al., 2019) highlights long-range contexts by aggregating multiple documents on a single incident. Additionally, each MultiNews item includes a human-written summary, providing even stronger long-range dependencies and better performance. Calculating loss on the summary of MultiNews leads to significantly better performance, with a 60% increase in retrieval accuracy and a 0.98 decrease in perplexity.

Furthermore, using summaries generated by the original dense model as supervision promotes higher alignment between its own attention patterns and the text supervision. It improves performance compared to potentially inconsistent human summaries, as shown in the last two rows of Table 2.

6 EXPERIMENT

6.1 SETUPS

We brief the experiment setups here, with more details in Appendix A.

Baselines. We compare MoA with state-of-the-art static and dynamic sparse attention methods, including StreamingLLM (Xiao et al., 2024c), InfLLM (Xiao et al., 2024a) and H2O (Zhang et al., 2023). We define the *density* of an LLM as the ratio of the average in-memory KV-Cache length to

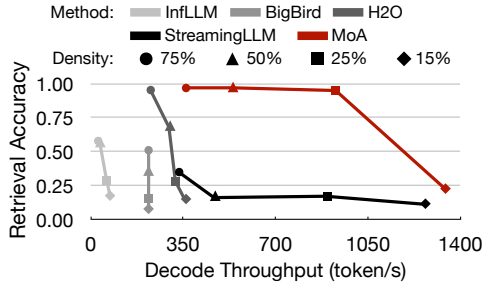


Figure 4: Accuracy-throughput trade-offs of various attention methods at different densities, tested on Vicuna-7B with 8k input length using one A100-80GB GPU on the LongEval dataset.

Mask Design	Retrieval Acc.		PPL	
	8k	16k	8k	12k
Uniform	0.25	0.15	4.89	5.19
+Hetero. Layers	0.31	0.26	4.55	4.85
+Hetero. Heads	0.95	0.41	3.96	4.30
+Elastic	0.98	0.43	3.96	4.29

Table 3: Ablation study on search space with consistent 25% density, progressively introducing heterogeneity in layers, heads, and elastic rules. Evaluations are done with retrieval accuracy and perplexity.

the sequence length during the sparse decode stage. Notably, in MoA and StreamingLLM, KV-Cache length equals the attention span during the sparse prefill stage. In contrast, H2O use dense prefill. Besides, H2O and InfLLM require additional computations to dynamically determine the KV-Cache.

Models and Benchmarks. We evaluate on vicuna-{7b, 13b}-v1.5-16k models (Chiang et al., 2023) from LMSys and Llama-3-{8b, 70b}-Instruct-262k models (AI, 2024) from Gradient AI. For long-context retrieval, we use LongEval (Li et al., 2023) to test key-value retrieval accuracy with 100 data items per length level. For long-context understanding, we use LV-Eval (Yuan et al., 2024) and LongBench (Bai et al., 2023), which include 11 and 13 sub-datasets, respectively. For coherence testing, we measure perplexity on four long datasets (Dasigi et al., 2021; Fabbri et al., 2019; Li & Roth, 2002; Hovy et al., 2001; Mohler et al., 2016) with diverse tasks. Unless otherwise specified, performance experiments are restricted to eight A100-80GB GPUs over a 24-hour period, with OOM (Out-Of-Memory) and OOT (Out-Of-Time) conditions noted. Efficiency experiments measure the decode throughput on a single A100-80GB GPU at maximum batch sizes of respective methods.

MoA Settings. We restrict the number of distinct rules to at most two per model layer to ensure inference-time efficiency. We profile MoA on MultiNews (Fabbri et al., 2019) with model summaries at 2k, 4k, and 8k lengths. The optimal compression plan is selected with the validation dataset at 12k. Each model uses the same plan across all benchmarks and lengths. The models are not fine-tuned.

6.2 ACCURACY-THROUGHPUT TRADE-OFF

Figure 4 shows that MoA advances the Pareto Front in context retrieval accuracy and decode throughput across varied densities. At the same densities, MoA notably enhances throughput by $1.6\times$ to $18.1\times$ compared to H2O and InfLLM, due to its efficient static attention design. The throughput even outperforms StreamingLLM thanks to our customized GPU kernel. Additionally, MoA achieves notably higher retrieval accuracies across all densities. We conduct extensive evaluations for MoA’s performance and efficiency on various benchmarks across context lengths from 4k to 256k and model sizes ranging from 7B to 70B in subsequent sections.

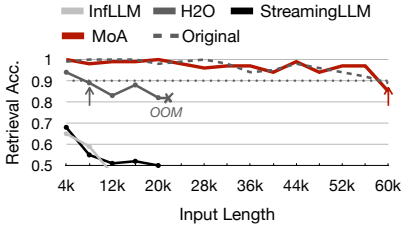
6.3 PERFORMANCE

MoA outperforms state-of-the-art sparse attention methods across various model sizes and benchmarks, achieving comparable performance to the original dense model at 50% density.

Long-Context Retrieval. As shown in Table 4, MoA demonstrates a maximum of 8% relative accuracy drop (calculated as $\max\{1 - \text{Acc}_{\text{MoA}} / \text{Acc}_{\text{Original}}\}$ across three lengths and LLMs), significantly less than the 87%, 58% and 44% for StreamingLLM, InfLLM and H2O. On average, the relative accuracy drop for MoA is under 1%, much less than others at 51%, 41% and 20%, respectively. Figure 5(a) shows that MoA retains over 90% retrieval accuracy up to 60k lengths, equaling the dense model’s effective context length. Note that it is done within 8k profiling and 12k validation. In contrast, the effective context lengths for H2O, InfLLM, and StreamingLLM are only 8k, <4k, and <4k, respectively. Appendix B.1.2 shows that MoA extends its effective context to approximately $3.9\times$ the average KV-Cache length.

Table 4: Comparative analysis of retrieval accuracy, LV-Eval scores, LongBench scores, and perplexity for various models with different attention methods. All sparse methods employ 50% density in decode stage. H2O uses dense prefill, while StreamingLLM, InfLLM and MoA use sparse prefill. InfLLM for 70B model is excluded due to OOT issues.

Model	Attention	Retrieve Acc. \uparrow			LV-Eval \uparrow	LongBench \uparrow	PPL \downarrow
		4k	8k	16k	16k	0-16k	8-12k
Vicuna-7B	Original	1.00	0.98	0.62	5.93	34.76	3.79
	H2O	0.86	0.68	0.35	5.42	33.59	3.94
	InfLLM	0.67	0.57	0.26	5.13	32.97	4.07
	StreamingLLM	0.43	0.16	0.08	4.72	31.84	4.48
	MoA	1.00	0.97	0.57	5.61	33.96	3.75
Vicuna-13B	Original	0.99	0.98	0.44	5.83	39.23	3.62
	H2O	0.88	0.76	0.28	5.66	38.13	3.80
	InfLLM	0.70	0.53	0.27	6.80	37.13	4.07
	StreamingLLM	0.65	0.49	0.33	5.43	32.13	4.10
	MoA	0.99	0.93	0.49	7.16	38.77	3.62
Llama3-8B	Original	0.99	0.99	0.97	17.49	43.69	4.52
	H2O	0.94	0.89	0.88	16.03	42.99	4.63
	InfLLM	0.65	0.59	0.37	14.44	42.43	4.68
	StreamingLLM	0.68	0.55	0.52	11.16	38.22	4.79
	MoA	0.99	1.00	1.00	17.46	42.97	4.49
Llama3-70B	Original	1.00	0.99	0.93	24.51	49.10	3.67
	H2O	0.93	0.91	OOM	OOM	OOM	OOM
	StreamingLLM	0.20	0.15	0.04	17.45	42.53	4.26
	MoA	1.00	1.00	0.94	23.65	47.79	3.75



(a) Retrieval accuracy and the effective context length (arrow).

Attention	Retrieve Acc. \uparrow				LV-Eval \uparrow		
	32k	64k	128k	256k	32k	64k	128k
Original	0.98	0.93	0.76	0.37	16.74	15.39	14.71
InfLLM	0.43	0.32	0.25	OOT	14.22	12.17	OOT
StreamingLLM	0.52	0.48	0.41	0.25	12.38	11.45	11.94
MoA	1.00	0.92	0.83	0.46	17.07	15.13	14.14

(b) Retrieval accuracy and LV-Eval score at longer lengths

Figure 5: Comparative analysis at extended sequence lengths with different attention methods using Llama3-8B model. All methods employ 50% density in both prefill and decode stages.

Long-Context Understanding. As shown in Table 4, MoA minimizes the maximum relative performance drop in LV-Eval and LongBench benchmarks to only 5% and 3%, respectively—much lower than the 36% and 18% experienced by StreamingLLM. H2O and InfLLM show maximum relative drops of 9%-17% and 3%-5% with higher efficiency costs. Similar trends show in perplexity tests, where MoA maintains less than 1% relative perplexity increase, while others exhibit 4%-13% increases. This trend holds for other densities, as shown in Appendices B.1.1 and B.1.3. Figure 9 and Table 8 further details the score with different tasks. MoA achieves comprehensive performance comparable to the original dense model, as well as H2O that requires higher efficiency cost. In contrast, StreamingLLM and InfLLM display inconsistent performance: it sometimes surpasses the original model in some tasks, while suffering noticeable degradation in others.

Longer-Context Generalization. By compressing within 12k lengths, MoA effectively generalizes to lengths of 32k-256k, as shown in Figure 5(b). At the extended lengths, MoA outperforms both InfLLM and StreamingLLM by 1.9 – 3.3 \times in retrieval accuracy and 1.2 – 1.4 \times in LV-Eval scores, demonstrating comparable performance to the original dense model.

Table 5: Runtime efficiency of different methods on Vicuna-7B and 13B models. Efficiency improvements of MoA are ablated with four factors. All sparse attention methods use 50% density. Decode throughput (tokens per second) evaluated at the maximum batch capacity of an A100-80GB GPU.

Model	Framework	Attention	4k		8k		16k	
			Batch	Throughput	Batch	Throughput	Batch	Throughput
7B	vLLM	PagedAttention	30	628.8	15	323.0	8	145.5
	FlexGen	H2O	20	754.9	6	296.3	1	51.7
	HuggingFace	InfLLM	15	62.0	10	37.5	6	19.2
	HuggingFace	StreamingLLM	50	945.1	25	467.3	12	232.0
	HuggingFace	FlashAttention2	30	134.6	15	66.9	8	32.9
		+Static KV-Cache	30	496.1	15	219.5	8	91.6
		+Reduced Attention	30	722.5	15	369.9	8	178.3
		+Increased Batch	50	897.7	25	436.7	12	206.4
		+Kernel (=MoA)	50	1099.0	25	535.7	12	257.3
13B	vLLM	PagedAttention	16	314.8	8	160.5	4	71.1
	FlexGen	H2O	12	330.2	4	138.2	1	37.4
	HuggingFace	InfLLM	8	30.3	5	17.63	3	11.3
	HuggingFace	StreamingLLM	28	478.4	14	241.2	7	116.5
	HuggingFace	FlashAttention2	16	81.3	8	40.8	4	19.8
		+Static KV-Cache	16	264.6	8	111.3	4	62.2
		+Reduced Attention	16	329.6	8	156.4	4	87.3
		+Increased Batch	28	471.5	14	222.6	7	108.3
		+Kernel (=MoA)	28	550.9	14	267.6	7	132.3

Ablation Study. We evaluate the performance impact of different sparse mask search spaces in Table 3. Starting with a basic uniform mask, we observe significant enhancements by sequentially introducing heterogeneity: layers first, then heads, and finally elastic rules.

6.4 EFFICIENCY

MoA shows high runtime efficiency with a manageable one-time compression overhead.

Runtime Efficiency. Table 5 compares the runtime efficiency of MoA over various attention methods and LLM frameworks, with the ablation of efficiency improvements brought by each design factor of MoA. At 50% density, MoA boosts the decode throughput by $6.6\times$ to $8.2\times$ compared to FlashAttention2. It outperforms H2O and InfLLM with $1.2\times$ to $4.0\times$ decode throughput improvements. Even compared to the highly system-level optimized vLLM framework (Kwon et al., 2023), MoA still achieves a $1.7\times$ to $1.9\times$ throughput increase. MoA also reduces total GPU memory by $1.2\times$ to $1.4\times$, are detailed in Appendix B.2. This throughput gain results from four main factors: static-sized KV-Cache during generation ($\approx 3.0\times$); reduced attention computations due to sparsity ($\approx 1.5\times$); increased batch sizes enabled by smaller KV-Cache memory ($\approx 1.4\times$); and our CUDA-implemented GPU kernel for MoA heterogeneous attention ($\approx 1.2\times$).

Compression Pipeline Efficiency. MoA completes the automatic compression pipeline for the Vicuna-7B and 13B models within two hours. For the larger Llama3-70B model, the process requires 8.5 hours of real-time and 34.7 hours of GPU time. Details for each compression step overhead are in Appendix B.2.2.

6.5 RULES DISCOVERED BY MOA

We investigate MoA’s elastic rules for each head. As shown in Figure 10, masks in the initial and middle layers exhibit high density, aligning with the conclusions from previous research on LLM’s intrinsic dimensions (Valeriani et al., 2023) and layer sensitivities (Yuan et al., 2023). Conversely, in the final layers, most heads require low density, while few need high density. Figure 11 shows that layers with lower average mask density typically display a wider range of densities among heads, confirming the need for heterogeneity within the same layer. Further details and quantified insights are presented in Appendix C.

7 CONCLUSION AND FUTURE WORK

MoA automates the selection of heterogeneous elastic masks for each attention head and input length, significantly extending the effective context length of LLMs by $3.9\times$. It enhances retrieval accuracy by $1.5\times$ to $7.1\times$ over uniform sparse attention method and increases throughput to over $6\times$ at 50% average density, maintaining performance on par with dense models in rigorous benchmarks.

Limitations and Future Work. Under an extremely low-density budget, MoA fails to maintain good performance. Designing a dynamic MoA method has the potential to address this issue, which we leave for future work. Using non-linear elastic rules with bounded attention spans is also worth exploring. Additionally, MoA’s profiling method can be adapted to evaluate the influence of weights and other activations, facilitating other compression methods such as weight and activation quantization (Lin et al., 2023; Xiao et al., 2024b; Li et al., 2024b).

ACKNOWLEDGEMENT

This work was supported by National Natural Science Foundation of China (No. 62325405, 62104128, U19B2019, U21B2031, 61832007, 62204164), Tsinghua EE Xilinx AI Research Fund, and Beijing National Research Center for Information Science and Technology (BNRist).

REFERENCES

- Meta AI. Introducing llama 3: Meta’s latest large language model. <https://ai.meta.com/blog/meta-llama-3/>, 2024. Accessed: 2024-05-17.
- Reza Yazdani Aminabadi, Samyam Rajbhandari, Minjia Zhang, Ammar Ahmad Awan, Cheng Li, Du Li, Elton Zheng, Jeff Rasley, Shaden Smith, Olatunji Ruwase, and Yuxiong He. Deepspeed-inference: Enabling efficient inference of transformer models at unprecedented scale. *SC22: International Conference for High Performance Computing, Networking, Storage and Analysis*, pp. 1–15, 2022. URL <https://api.semanticscholar.org/CorpusID:250243681>.
- Sotiris Anagnostidis, Dario Pavllo, Luca Biggio, Lorenzo Noci, Aurélien Lucchi, and Thomas Hofmann. Dynamic context pruning for efficient and interpretable autoregressive transformers. *ArXiv*, abs/2305.15805, 2023. URL <https://api.semanticscholar.org/CorpusID:258888224>.
- Yushi Bai, Xin Lv, Jiajie Zhang, Hongchang Lyu, Jiankai Tang, Zhidian Huang, Zhengxiao Du, Xiao Liu, Aohan Zeng, Lei Hou, Yuxiao Dong, Jie Tang, and Juanzi Li. Longbench: A bilingual, multitask benchmark for long context understanding, 2023.
- Iz Beltagy, Matthew E Peters, and Arman Cohan. Longformer: The long-document transformer. *arXiv preprint arXiv:2004.05150*, 2020.
- Tom Brown, Benjamin Mann, Nick Ryder, Melanie Subbiah, Jared D Kaplan, Prafulla Dhariwal, Arvind Neelakantan, Pranav Shyam, Girish Sastry, Amanda Askell, et al. Language models are few-shot learners. *Advances in neural information processing systems*, 33:1877–1901, 2020.
- Shouyuan Chen, Sherman Wong, Liangjian Chen, and Yuandong Tian. Extending context window of large language models via positional interpolation. *ArXiv*, abs/2306.15595, 2023. URL <https://api.semanticscholar.org/CorpusID:259262376>.
- Wei-Lin Chiang, Zhuohan Li, Zi Lin, Ying Sheng, Zhanghao Wu, Hao Zhang, Lianmin Zheng, Siyuan Zhuang, Yonghao Zhuang, Joseph E. Gonzalez, Ion Stoica, and Eric P. Xing. Vicuna: An open-source chatbot impressing gpt-4 with 90%* chatgpt quality, March 2023. URL <https://lmsys.org/blog/2023-03-30-vicuna/>.
- Rewon Child, Scott Gray, Alec Radford, and Ilya Sutskever. Generating long sequences with sparse transformers. *arXiv preprint arXiv:1904.10509*, 2019.
- Krzysztof Marcin Choromanski, Valerii Likhoshesterov, David Dohan, Xingyou Song, Andreea Gane, Tamas Sarlos, Peter Hawkins, Jared Quincy Davis, Afroz Mohiuddin, Lukasz Kaiser, et al. Rethinking attention with performers. In *International Conference on Learning Representations*, 2020.
- Together Computer. Redpajama: An open source recipe to reproduce llama training dataset, April 2023. URL <https://github.com/togethercomputer/RedPajama-Data>.
- Tri Dao. Flashattention-2: Faster attention with better parallelism and work partitioning. *ArXiv*, abs/2307.08691, 2023. URL <https://api.semanticscholar.org/CorpusID:259936734>.
- Tri Dao, Daniel Y. Fu, Stefano Ermon, Atri Rudra, and Christopher Ré. FlashAttention: Fast and memory-efficient exact attention with IO-awareness. In *Advances in Neural Information Processing Systems*, 2022.
- Rocktim Jyoti Das, Liqun Ma, and Zhiqiang Shen. Beyond size: How gradients shape pruning decisions in large language models. *arXiv preprint arXiv:2311.04902*, 2023.
- Pradeep Dasigi, Kyle Lo, Iz Beltagy, Arman Cohan, Noah A. Smith, and Matt Gardner. A dataset of information-seeking questions and answers anchored in research papers. *ArXiv*, abs/2105.03011, 2021. URL <https://api.semanticscholar.org/CorpusID:234093776>.
- Jacob Devlin, Ming-Wei Chang, Kenton Lee, and Kristina Toutanova. Bert: Pre-training of deep bidirectional transformers for language understanding. *arXiv preprint arXiv:1810.04805*, 2018.

-
- Alexander R. Fabbri, Irene Li, Tianwei She, Suyi Li, and Dragomir R. Radev. Multi-news: A large-scale multi-document summarization dataset and abstractive hierarchical model. In *Annual Meeting of the Association for Computational Linguistics*, 2019. URL <https://api.semanticscholar.org/CorpusID:174799390>.
- Aosong Feng, Irene Li, Yuang Jiang, and Rex Ying. Diffuser: Efficient transformers with multi-hop attention diffusion for long sequences. *arXiv preprint arXiv:2210.11794*, 2022.
- Suyu Ge, Yunan Zhang, Liyuan Liu, Minjia Zhang, Jiawei Han, and Jianfeng Gao. Model tells you what to discard: Adaptive kv cache compression for llms. *ArXiv*, abs/2310.01801, 2023. URL <https://api.semanticscholar.org/CorpusID:263609075>.
- Albert Gu and Tri Dao. Mamba: Linear-time sequence modeling with selective state spaces. *ArXiv*, abs/2312.00752, 2023. URL <https://api.semanticscholar.org/CorpusID:265551773>.
- Sylvain Gugger, Lysandre Debut, Thomas Wolf, Philipp Schmid, Zachary Mueller, Sourab Mangrulkar, Marc Sun, and Benjamin Bossan. Accelerate: Training and inference at scale made simple, efficient and adaptable. <https://github.com/huggingface/accelerate>, 2022.
- Gurobi Optimization, LLC. Gurobi Optimizer Reference Manual, 2023. URL <https://www.gurobi.com>.
- Tae Jun Ham et al. A³: Accelerating attention mechanisms in neural networks with approximation. In *HPCA*, pp. 328–341. IEEE, 2020.
- Tae Jun Ham et al. Elsa: Hardware-software co-design for efficient, lightweight self-attention mechanism in neural networks. In *ISCA*, pp. 692–705. IEEE, 2021.
- Chi Han, Qifan Wang, Wenhan Xiong, Yu Chen, Heng Ji, and Sinong Wang. Lm-infinite: Simple on-the-fly length generalization for large language models. *arXiv preprint arXiv:2308.16137*, 2023.
- Eduard Hovy, Laurie Gerber, Ulf Hermjakob, Chin-Yew Lin, and Deepak Ravichandran. Toward semantics-based answer pinpointing. In *Proceedings of the First International Conference on Human Language Technology Research*, 2001. URL <https://www.aclweb.org/anthology/H01-1069>.
- Cheng Jiang, Ranjun Li, Zhuoyi Zhang, and Yu Shen. Pushing gradient towards zero: A novel pruning method for large language models, 2023.
- Praneeth Kacham, Vahab S. Mirrokni, and Peilin Zhong. Polysketchformer: Fast transformers via sketches for polynomial kernels. *ArXiv*, abs/2310.01655, 2023. URL <https://api.semanticscholar.org/CorpusID:263609343>.
- Sehoon Kim, Coleman Hooper, Amir Gholami, Zhen Dong, Xiuyu Li, Sheng Shen, Michael W Mahoney, and Kurt Keutzer. Squeezellm: Dense-and-sparse quantization. *arXiv preprint arXiv:2306.07629*, 2023.
- Nikita Kitaev, Łukasz Kaiser, and Anselm Levskaya. Reformer: The efficient transformer. *arXiv preprint arXiv:2001.04451*, 2020.
- Woosuk Kwon, Zhuohan Li, Siyuan Zhuang, Ying Sheng, Lianmin Zheng, Cody Hao Yu, Joseph E. Gonzalez, Haoteng Zhang, and Ion Stoica. Efficient memory management for large language model serving with pagedattention. *Proceedings of the 29th Symposium on Operating Systems Principles*, 2023. URL <https://api.semanticscholar.org/CorpusID:261697361>.
- Je-Yong Lee, Donghyun Lee, Genghan Zhang, Mo Tiwari, and Azalia Mirhoseini. Cats: Contextually-aware thresholding for sparsity in large language models. *arXiv preprint arXiv:2404.08763*, 2024.
- Dacheng Li, Rulin Shao, Anze Xie, Ying Sheng, Lianmin Zheng, Joseph E. Gonzalez, Ion Stoica, Xuezhe Ma, and Hao Zhang. How long can open-source llms truly promise on context length?, June 2023. URL <https://lmsys.org/blog/2023-06-29-longchat>.

-
- Shiyao Li, Xuefei Ning, Ke Hong, Tengxuan Liu, Luning Wang, Xiuhong Li, Kai Zhong, Guohao Dai, Huazhong Yang, and Yu Wang. Llm-mq: Mixed-precision quantization for efficient llm deployment. *NeurIPS Workshop*, 2024a.
- Shiyao Li, Xuefei Ning, Luning Wang, Tengxuan Liu, Xiangsheng Shi, Shengen Yan, Guohao Dai, Huazhong Yang, and Yu Wang. Evaluating quantized large language models. *arXiv preprint arXiv:2402.18158*, 2024b.
- Xin Li and Dan Roth. Learning question classifiers. In *COLING 2002: The 19th International Conference on Computational Linguistics*, 2002. URL <https://www.aclweb.org/anthology/C02-1150>.
- Yuhong Li, Tianle Cai, Yi Zhang, De huai Chen, and Debadeepta Dey. What makes convolutional models great on long sequence modeling? *ArXiv*, abs/2210.09298, 2022. URL <https://api.semanticscholar.org/CorpusID:252917984>.
- Ji Lin, Jiaming Tang, Haotian Tang, Shang Yang, Xingyu Dang, and Song Han. Awq: Activation-aware weight quantization for llm compression and acceleration. *arXiv preprint arXiv:2306.00978*, 2023.
- Zichang Liu, Aditya Desai, Fangshuo Liao, Weitao Wang, Victor Xie, Zhaozhuo Xu, Anastasios Kyrillidis, and Anshumali Shrivastava. Scissorhands: Exploiting the persistence of importance hypothesis for llm kv cache compression at test time. *ArXiv*, abs/2305.17118, 2023a. URL <https://api.semanticscholar.org/CorpusID:258947558>.
- Zichang Liu, Jue Wang, Tri Dao, Tianyi Zhou, Binhang Yuan, Zhao Song, Anshumali Shrivastava, Ce Zhang, Yuandong Tian, Christopher Re, et al. Deja vu: Contextual sparsity for efficient llms at inference time. In *International Conference on Machine Learning*, pp. 22137–22176. PMLR, 2023b.
- Liqiang Lu, Yicheng Jin, Hangrui Bi, Zizhang Luo, Peng Li, Tao Wang, and Yun Liang. Sanger: A co-design framework for enabling sparse attention using reconfigurable architecture. In *MICRO-54: 54th Annual IEEE/ACM International Symposium on Microarchitecture*, MICRO '21, pp. 977–991, New York, NY, USA, 2021. Association for Computing Machinery. ISBN 9781450385572. doi: 10.1145/3466752.3480125. URL <https://doi.org/10.1145/3466752.3480125>.
- Xin Men, Mingyu Xu, Qingyu Zhang, Bingning Wang, Hongyu Lin, Yaojie Lu, Xianpei Han, and Weipeng Chen. Shortgpt: Layers in large language models are more redundant than you expect. *ArXiv*, abs/2403.03853, 2024. URL <https://api.semanticscholar.org/CorpusID:268253513>.
- Michael Mohler, Mary Brunson, Bryan Rink, and Marc Tomlinson. Introducing the LCC metaphor datasets. In Nicoletta Calzolari, Khalid Choukri, Thierry Declerck, Sara Goggi, Marko Grobelnik, Bente Maegaard, Joseph Mariani, Helene Mazo, Asuncion Moreno, Jan Odijk, and Stelios Piperidis (eds.), *Proceedings of the Tenth International Conference on Language Resources and Evaluation (LREC'16)*, pp. 4221–4227, Portorož, Slovenia, May 2016. European Language Resources Association (ELRA). URL <https://aclanthology.org/L16-1668>.
- Matteo Pagliardini, Daniele Paliotta, Martin Jaggi, and Francois Fleuret. Faster causal attention over large sequences through sparse flash attention. *ArXiv*, abs/2306.01160, 2023. URL <https://api.semanticscholar.org/CorpusID:259063695>.
- Biswajit Paria, Kirthevasan Kandasamy, and Barnabás Póczos. A flexible framework for multi-objective bayesian optimization using random scalarizations. In *Conference on Uncertainty in Artificial Intelligence*, 2018. URL <https://api.semanticscholar.org/CorpusID:53034523>.
- Adam Paszke, Sam Gross, Francisco Massa, Adam Lerer, James Bradbury, Gregory Chanan, Trevor Killeen, Zeming Lin, Natalia Gimelshein, Luca Antiga, et al. Pytorch: An imperative style, high-performance deep learning library. *Advances in neural information processing systems*, 32, 2019.

-
- Bo Peng, Eric Alcaide, Quentin G. Anthony, Alon Albalak, Samuel Arcadinho, Stella Biderman, Huanqi Cao, Xin Cheng, Michael Chung, Matteo Grella, G. Kranthikiran, Xuming He, Haowen Hou, Przemyslaw Kazienko, Jan Kocoń, Jiaming Kong, Bartłomiej Koptyra, Hayden Lau, Krishna Sri Ipsit Mantri, Ferdinand Mom, Atsushi Saito, Xiangru Tang, Bolun Wang, Johan Sokrates Wind, Stansilaw Wozniak, Ruichong Zhang, Zhenyuan Zhang, Qihang Zhao, Peng Zhou, Jian Zhu, and Rui Zhu. Rwk: Reinventing rnns for the transformer era. In *Conference on Empirical Methods in Natural Language Processing*, 2023. URL <https://api.semanticscholar.org/CorpusID:258832459>.
- Hao Peng, Nikolaos Pappas, Dani Yogatama, Roy Schwartz, Noah A. Smith, and Lingpeng Kong. Random feature attention. *ArXiv*, abs/2103.02143, 2021. URL <https://api.semanticscholar.org/CorpusID:232105052>.
- Michael Poli, Stefano Massaroli, Eric Nguyen, Daniel Y Fu, Tri Dao, Stephen Baccus, Yoshua Bengio, Stefano Ermon, and Christopher Ré. Hyena hierarchy: Towards larger convolutional language models. *arXiv preprint arXiv:2302.10866*, 2023.
- Zheng Qu, Liu Liu, Fengbin Tu, Zhaodong Chen, Yufei Ding, and Yuan Xie. Dota: Detect and omit weak attentions for scalable transformer acceleration. In *Proceedings of the 27th ACM International Conference on Architectural Support for Programming Languages and Operating Systems*, ASPLOS ’22, pp. 14–26, New York, NY, USA, 2022. Association for Computing Machinery. ISBN 9781450392051. doi: 10.1145/3503222.3507738. URL <https://doi.org/10.1145/3503222.3507738>.
- Aurko Roy, Mohammad Saffar, Ashish Vaswani, and David Grangier. Efficient content-based sparse attention with routing transformers. *Transactions of the Association for Computational Linguistics*, 9:53–68, 2021.
- Jay Shah, Ganesh Bikshandi, Ying Zhang, Vijay Thakkar, Pradeep Ramani, and Tri Dao. Flashattention-3: Fast and accurate attention with asynchrony and low-precision. *arXiv preprint arXiv:2407.08608*, 2024.
- Ying Sheng, Lianmin Zheng, Binhang Yuan, Zhuohan Li, Max Ryabinin, Daniel Y. Fu, Zhiqiang Xie, Beidi Chen, Clark W. Barrett, Joseph Gonzalez, Percy Liang, Christopher Ré, Ion Stoica, and Ce Zhang. High-throughput generative inference of large language models with a single gpu. In *International Conference on Machine Learning*, 2023. URL <https://api.semanticscholar.org/CorpusID:257495837>.
- Han Shi, Jiahui Gao, Xiaozhe Ren, Hang Xu, Xiaodan Liang, Zhenguo Li, and James Tin-Yau Kwok. Sparsebert: Rethinking the importance analysis in self-attention. In *International Conference on Machine Learning*, pp. 9547–9557. PMLR, 2021.
- Yutao Sun, Li Dong, Shaohan Huang, Shuming Ma, Yuqing Xia, Jilong Xue, Jianyong Wang, and Furu Wei. Retentive network: A successor to transformer for large language models. *ArXiv*, abs/2307.08621, 2023. URL <https://api.semanticscholar.org/CorpusID:259937453>.
- Jiaming Tang, Yilong Zhao, Kan Zhu, Guangxuan Xiao, Baris Kasikci, and Song Han. Quest: Query-aware sparsity for efficient long-context llm inference. *arXiv preprint arXiv:2406.10774*, 2024.
- Yi Tay, Mostafa Dehghani, Dara Bahri, and Donald Metzler. Efficient transformers: A survey. *ACM Comput. Surv.*, 55(6), dec 2022. ISSN 0360-0300. doi: 10.1145/3530811. URL <https://doi.org/10.1145/3530811>.
- Hugo Touvron, Thibaut Lavril, Gautier Izacard, Xavier Martinet, Marie-Anne Lachaux, Timothée Lacroix, Baptiste Rozière, Naman Goyal, Eric Hambro, Faisal Azhar, et al. Llama: Open and efficient foundation language models. *arXiv preprint arXiv:2302.13971*, 2023.
- Szymon Tworkowski, Konrad Staniszewski, Mikolaj Pacek, Yuhuai Wu, Henryk Michalewski, and Piotr Milo’s. Focused transformer: Contrastive training for context scaling. *ArXiv*, abs/2307.03170, 2023. URL <https://api.semanticscholar.org/CorpusID:259360592>.

-
- Lucrezia Valeriani, Diego Doimo, Francesca Cuturello, Alessandro Laio, Alessio Ansuini, and Alberto Cazzaniga. The geometry of hidden representations of large transformer models. *ArXiv*, abs/2302.00294, 2023. URL <https://api.semanticscholar.org/CorpusID:256459698>.
- Ashish Vaswani, Noam Shazeer, Niki Parmar, Jakob Uszkoreit, Llion Jones, Aidan N Gomez, Łukasz Kaiser, and Illia Polosukhin. Attention is all you need. *Advances in neural information processing systems*, 30, 2017.
- Zhongwei Wan, Xin Wang, Che Liu, Samiul Alam, Yu Zheng, Jiachen Liu, Zhongnan Qu, Shen Yan, Yi Zhu, Quanlu Zhang, Mosharaf Chowdhury, and Mi Zhang. Efficient large language models: A survey. *ArXiv*, abs/2312.03863, 2023. URL <https://api.semanticscholar.org/CorpusID:266044196>.
- Hanrui Wang, Zhekai Zhang, and Song Han. Spatten: Efficient sparse attention architecture with cascade token and head pruning. In *2021 IEEE International Symposium on High-Performance Computer Architecture (HPCA)*, pp. 97–110. IEEE, 2021.
- Sinong Wang, Belinda Z Li, Madian Khabsa, Han Fang, and Hao Ma. Linformer: Self-attention with linear complexity. *arXiv preprint arXiv:2006.04768*, 2020.
- Wenhao Wu, Yizhong Wang, Guangxuan Xiao, Hao Peng, and Yao Fu. Retrieval head mechanistically explains long-context factuality. *arXiv preprint arXiv:2404.15574*, 2024.
- Chaojun Xiao, Pengl Zhang, Xu Han, Guangxuan Xiao, Yankai Lin, Zhengyan Zhang, Zhiyuan Liu, Song Han, and Maosong Sun. Infilmm: Unveiling the intrinsic capacity of llms for understanding extremely long sequences with training-free memory. *arXiv preprint arXiv:2402.04617*, 2024a.
- Guangxuan Xiao, Ji Lin, Mickael Seznec, Hao Wu, Julien Demouth, and Song Han. Smoothquant: Accurate and efficient post-training quantization for large language models, 2024b.
- Guangxuan Xiao, Yuandong Tian, Beidi Chen, Song Han, and Mike Lewis. Efficient streaming language models with attention sinks. *The Twelfth International Conference on Learning Representations*, 2024c.
- Tao Yuan, Xuefei Ning, Dong Zhou, Zhijie Yang, Shiyao Li, Minghui Zhuang, Zheyue Tan, Zhuyu Yao, Dahua Lin, Boxun Li, Guohao Dai, Shengen Yan, and Yu Wang. Lv-eval: A balanced long-context benchmark with 5 length levels up to 256k, 2024.
- Zhihang Yuan, Yuzhang Shang, Yue Song, Qiang Wu, Yan Yan, and Guangyu Sun. Asvd: Activation-aware singular value decomposition for compressing large language models. *ArXiv*, abs/2312.05821, 2023. URL <https://api.semanticscholar.org/CorpusID:266162471>.
- Yv Haimen Yv, Leon S. Lasdon, and Dang Da. On a bicriterion formation of the problems of integrated system identification and system optimization. *IEEE Transactions on Systems, Man, and Cybernetics*, pp. 296–297, 1971. URL <https://api.semanticscholar.org/CorpusID:125851974>.
- Manzil Zaheer, Guru Guruganesh, Kumar Avinava Dubey, Joshua Ainslie, Chris Alberti, Santiago Ontanon, Philip Pham, Anirudh Ravula, Qifan Wang, Li Yang, et al. Big bird: Transformers for longer sequences. *Advances in neural information processing systems*, 33:17283–17297, 2020.
- Susan Zhang, Stephen Roller, Naman Goyal, Mikel Artetxe, Moya Chen, Shuohui Chen, Christopher Dewan, Mona T. Diab, Xian Li, Xi Victoria Lin, Todor Mihaylov, Myle Ott, Sam Shleifer, Kurt Shuster, Daniel Simig, Punit Singh Koura, Anjali Sridhar, Tianlu Wang, and Luke Zettlemoyer. Opt: Open pre-trained transformer language models. *ArXiv*, abs/2205.01068, 2022. URL <https://api.semanticscholar.org/CorpusID:248496292>.
- Zhenyu (Allen) Zhang, Ying Sheng, Tianyi Zhou, Tianlong Chen, Lianmin Zheng, Ruisi Cai, Zhao Song, Yuandong Tian, Christopher Ré, Clark W. Barrett, Zhangyang Wang, and Beidi Chen. H2o: Heavy-hitter oracle for efficient generative inference of large language models. *ArXiv*, abs/2306.14048, 2023. URL <https://api.semanticscholar.org/CorpusID:259263947>.

Zixuan Zhou, Xuefei Ning, Ke Hong, Tianyu Fu, Jiaming Xu, Shiyao Li, Yuming Lou, Luning Wang, Zhihang Yuan, Xiuhong Li, Shengen Yan, Guohao Dai, Xiao-Ping Zhang, Yuhan Dong, and Yu Wang. A survey on efficient inference for large language models. *ArXiv*, abs/2404.14294, 2024.
URL <https://api.semanticscholar.org/CorpusID:269293007>.

A DETAILED EXPERIMENT SETUP

A.1 MAIN SETUP

Baselines. In the setup for our experiment, we adhere to specific configurations outlined in the respective papers. In the case of In StreamingLLM (Xiao et al., 2024c), the initial four tokens remain unmasked, serving as the attention sink, except for the 70b model in Table 4 and the super long setting in Figure 5, where we use 64 tokens as the attention sink. For InfLLM (Xiao et al., 2024a), we adhere to the original configuration by maintaining the same local window size and selected memory size, using 128 initial tokens as specified in their setup. For H2O (Zhang et al., 2023), we ensure the same number of heavy hitter tokens and recent tokens. Note that H2O uses dense prefill since it relies on the column sum of the attention matrix to calculate the importance of every token for KV-Cache eviction. StreamingLLM, InfLLM and MoA use sparse prefill.

Models and Benchmarks. Since vicuna-7b-v1.5-16k and vicuna-13b-v1.5-16k (Chiang et al., 2023) can only take in 16k context length, we use the 16k split of LV-Eval benchmark (Yuan et al., 2024), truncating the input to 15500 for model input in Table 4. For the LongBench benchmark (Bai et al., 2023), we use the LongBench-E split, which features a balanced number of data items at every length level. The LongBench dataset is segmented into ranges of 0-4k, 4-8k, and 8k+ tokens. We test each split using the input length truncation thresholds of 3,500, 7,500, and 15,500 tokens, respectively.

Perplexity Evaluation. We construct a comprehensive yet concise test set by sampling 50×4 data items for each length level from the test split of four long-context understanding datasets: Qasper (Dasigi et al., 2021), MultiNew (Fabbri et al., 2019), TREC (Li & Roth, 2002; Hovy et al., 2001) and LCC (Mohler et al., 2016), representing the question answering, summarization, few-shot learning, and code completion abilities of the LLM. Following LongBench, the data items are organized as question-answer pairs. The questions and answers are written by humans and come with the dataset. The perplexity is calculated solely on the answer part of the data, demonstrating the model’s coherence in responding to user requests.

Validation Dataset. The validation dataset is used to select the optimal compression plan among the Pareto front solutions during the optimization step. The validation dataset is similarly constructed as the perplexity test dataset, but on the respective validation split of the datasets. 50×4 data items are sampled from the same four long-context understanding datasets: Qasper (Dasigi et al., 2021), MultiNew (Fabbri et al., 2019), TREC (Li & Roth, 2002; Hovy et al., 2001) and LCC (Mohler et al., 2016). The additional 50 data items from the LongEval (Li et al., 2023) dataset are also added to validate the retrieval ability. For the datasets that do not contain the validation split, namely TREC, MultiNews and LCC, we sample from the test split and ensure different data items with the perplexity evaluation dataset.

MoA Settings. MoA uses the block sparse attention pattern with a block size of 64, where each grid depicted in Figure 3(a) represents a block. The first block of tokens is not masked as the attention sink. For the profile stage, we use the MultiNews (Fabbri et al., 2019) calibration dataset with model response as supervision, as described in Section 5. We use 50×3 data items at 2k, 4k, 8k lengths. The data items are padded to their corresponding length level in order to ensure a unified shape of attention influence tensors for each length level. We adopt block granularity during the profiling stage, calculating the average attention influence within each block to represent the block’s overall influence. The optimization is done with the multi-objective optimization at the same set of lengths. We limit the number of distinct rules to at most two per model layer to ensure inference-time efficiency. Among the Pareto front solutions, we select the one with the lowest perplexity on the validation dataset of length 12k.

A.2 EFFICIENCY EXPERIMENT SETUP

We test the efficiency of different frameworks using a single NVIDIA A100-SXM4-80GB GPU. To improve the runtime profiling accuracy, we first run five forward passes as warmups. Then we use `torch.CudaEvent` to calculate the runtime for each method. Our experiments are structured around three scenarios: including prefilling 3k tokens and decoding 1k tokens; prefilling 6k tokens and decoding 2k tokens; prefilling 12k tokens and decoding 4k tokens. The labels are marked by the total sequence length, which equals prefill length plus decode length.

For MoA, The implementation is based on Huggingface Transformers. During the prefill stage, we use the sparse CUDA kernel designed by us with block size 64. During the decode stage, we modify the KV-Cache implementation to support our heterogeneous elastic rules. Thanks to our fixed sliding-window span during the decode stage, we simply replace the old KV-Cache that exceeds the span with the latest KV-Cache. Our custom decoding CUDA kernel then handles KV-Cache with varying lengths across different attention heads during the decoding process.

For H2O, we use its official efficient implementation, which is based on Flexgen (Sheng et al., 2023). Note that H2O uses dense prefill since it relies on the column sum of the attention matrix to calculate the importance of every token for KV-Cache eviction, which requires the attention matrix to be explicitly calculated. It makes H2O’s prefill stage currently incompatible with kernel optimizations like FlashAttention. Therefore, H2O is easy to get OOM (Out-Of-Memory) with large prefill length and increased batch size.

In our efficiency tests across all frameworks, we implemented a simple optimization at the language modeling head (lm head) during the prefill stage. Specifically, after the final layer of the transformers, we compute the logits—these are the raw outputs that are transformed into probabilities—for only the last token. This selective computation avoids generating these probabilities for preceding tokens, substantially reducing both computational overhead and memory usage. We also set the environment variable `PYTORCH_CUDA_ALLOC_CONF` to be `expandable_segments:True` for Huggingface and MoA to mitigate memory fragmentation, allowing larger inference batch size.

Following the performance experiments, we use Vicuna-7B and Vicuna-13B for efficiency tests whenever possible. However, the official efficient implementation of H2O based on Flexgen only supports OPT (Zhang et al., 2022). Therefore, we use OPT-6.7b and OPT-13b models for H2O in Table 9 for comparison.

A.3 ABLATION STUDY SETUP

In the ablation study in Table 2 and Table 3, we use 25% density instead of the 50% used in the main experiment in Table 4. This decision is based on the observation that at a density of 50%, the performance of the various designs is quite similar, making it difficult to discern significant differences. In contrast, a lower density of 25% reveals more pronounced disparities between the designs, providing a clearer basis for comparison.

In the calibration dataset experiments in Table 2, we intentionally exclude the influence of the validation dataset. We avoid using the validation dataset by profile and optimize solely at 8k length, reducing the multi-objective optimization problem to a single-objective one with only one optimal compression plan instead of a set of Pareto fronts.

B ADDITIONAL EXPERIMENT RESULTS

B.1 PERFORMANCE

B.1.1 OVERALL PERFORMANCE

Table 6 shows the overall performance of MoA at a higher density of 75%. MoA shows improved performance over the baseline with the uniform attention baseline. The progressive change of performance with respect to different densities is also shown in Figure 7(b) and Figure 8

B.1.2 LONG-CONTEXT RETRIEVAL

We conduct a detailed experiment to test the retrieval ability of different attention methods across various attention spans and input lengths.

Figure 6 shows the detailed data for effective context length calculation. As shown in the figure, StreamingLLM can hardly maintain retrieval accuracy when the input length is beyond the attention span, while MoA can effectively extend the effective context length.

Following previous work (Chen et al., 2023; Tworowski et al., 2023), we quantify effective context length as the maximum input length where retrieval accuracy remains above a 90% threshold. As

Table 6: Comparative analysis of retrieval accuracy, LV-Eval scores, LongBench scores, and perplexity for various models with different attention methods. All methods employ 75% density in both prefill and decode stages.

Model	Attention	Retrieve Acc. \uparrow			LV-Eval \uparrow	LongBench \uparrow			PPL \downarrow
		4k	8k	16k		0-4k	4-8k	8-16k	
Vicuna-7B	StreamingLLM	0.91	0.35	0.09	4.30	36.39	32.44	31.04	3.92
	MoA	1.00	0.97	0.58	5.67	38.07	33.80	31.75	3.78
Vicuna-13B	StreamingLLM	0.73	0.81	0.37	5.65	36.77	34.65	33.43	3.70
	MoA	0.99	0.97	0.42	5.57	41.85	39.76	36.06	3.62
Llama3-8B	StreamingLLM	1.00	0.83	0.76	14.89	42.45	40.62	42.51	4.51
	MoA	0.99	1.00	0.93	15.61	43.51	43.16	43.58	4.53

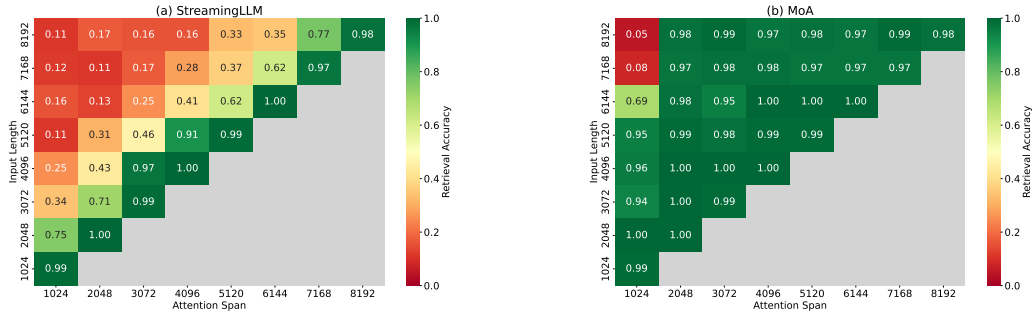


Figure 6: Retrieval accuracy of Vicuna-7B model using different attention methods across varying attention spans and input lengths. The X-axis shows different attention spans; the Y-axis shows different input lengths for the retrieval task. Subfigure (a) shows results for StreamingLLM, and subfigure (b) for MoA.

shown in Figure 7(a), StreamingLLM and H2O achieve effective context lengths of no more than 2k tokens beyond their attention spans. In contrast, MoA expands its effective context length to approximately $3.9\times$ its attention span before reaching up to the 12k limit of the original model. Figure 7(b) further shows that at a fixed input length of 8k, MoA reaches over 0.9 retrieval accuracy with just 25% density, whereas StreamingLLM and H2O require 100% and 75% density, respectively.

B.1.3 LONG-CONTEXT UNDERSTANDING

We conduct experiments with various densities on the LV-Eval benchmark (Yuan et al., 2024). As shown in Figure 8, MoA constantly outperforms the uniform static attention baseline StreamingLLM at various densities, demonstrating the effectiveness of our heterogeneous elastic rules.

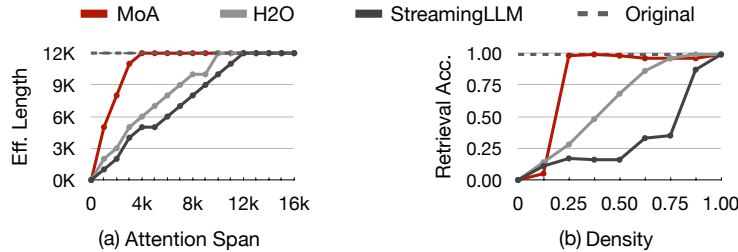


Figure 7: Retrieval accuracy tests on LongEval with Vicuna-7B. (a) Varies input lengths and densities to show effective context lengths across attention spans, (b) Set input length at 8k and show retrieval accuracy across different densities.

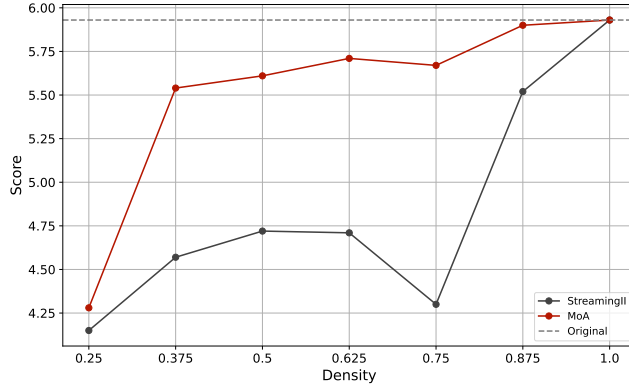


Figure 8: LV-Eval score of StreamingLLM and MoA at various densities on Vicuna-7B model.

Table 7: LongBench scores for various models with different attention methods. All methods employ 50% density in the decode stage.

Model	Attention	LongBench \uparrow		
		0-4k	4-8k	8-16k
Vicuna-7B	Original	37.91	33.82	32.54
	H2O	36.23	32.74	31.81
	InfLLM	35.23	33.54	30.15
	StreamingLLM	30.53	33.28	31.70
	MoA	37.04	32.90	31.94
Vicuna-13B	Original	42.25	39.52	35.93
	H2O	41.63	38.02	34.75
	InfLLM	39.36	37.66	34.36
	StreamingLLM	30.65	33.07	32.68
	MoA	41.73	38.88	35.69
Llama3-8B	Original	44.27	43.53	43.26
	H2O	43.46	43.01	42.50
	InfLLM	42.78	42.69	41.81
	StreamingLLM	37.20	38.02	39.43
	MoA	43.07	42.75	43.09
Llama3-70B	Original	50.70	48.05	48.55
	H2O	50.16	47.77	OOM
	StreamingLLM	45.14	42.40	40.04
	MoA	49.74	46.80	46.84

We detailed the respective scores for LongBench and LV-Eval in Table 7 and Table 8. The number in the bracket of Table 8 indicates the number of sub-datasets for the category.

B.2 EFFICIENCY

B.2.1 THROUGHPUT BREAKDOWN

In this section, we explain the decode throughput breakdown for MoA, compared to the baseline comprising Huggingface with FlashAttention2. The observed increase in throughput, as shown in Table 5, primarily stems from three aspects:

Table 8: Performance comparison across different models and attention methods with the LV-Eval dataset. The numbers in brackets indicate the number of sub-datasets for the category.

Model	Attention	Single-QA		Multi-QA		Retrieval
		w/o. Conf (2)	w. Conf (2)	w/o. Conf (3)	w. Conf (2)	w. Conf (2)
Vicuna-7B	Original	10.49	6.29	6.83	5.60	0.00
	H2O	9.16	6.20	6.44	4.80	0.00
	InfLLM	7.11	6.70	6.07	4.80	0.00
	StreamingLLM	7.54	5.90	5.98	3.56	0.00
	MoA	9.98	6.27	6.16	5.31	0.09
Vicuna-13B	Original	10.64	7.28	5.32	5.07	1.08
	H2O	9.53	6.54	5.25	5.36	1.83
	InfLLM	10.21	9.35	6.03	3.19	2.08
	StreamingLLM	9.05	5.86	5.37	3.19	3.70
	MoA	11.04	6.93	5.79	5.84	6.88
Llama3-8B	Original	34.05	19.51	11.41	17.70	7.84
	H2O	28.52	17.05	11.11	15.98	9.95
	InfLLM	24.94	17.75	10.61	14.80	6.04
	StreamingLLM	20.21	9.57	8.14	9.36	10.03
	MoA	32.98	20.53	10.65	17.57	8.98
Llama3-70B	Original	44.44	25.02	16.71	22.86	17.43
	StreamingLLM	26.63	14.22	14.04	14.70	19.38
	MoA	42.44	23.58	15.75	21.27	19.19

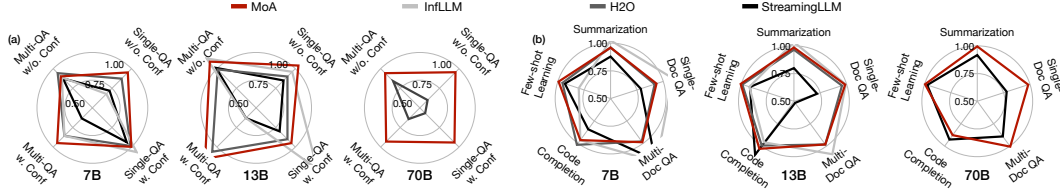


Figure 9: (a) LV-Eval and (b) LongBench scores for different attention methods at 50% density, tested on Vicuna-7B, 13B and Llama3-70B models. Scores normalized against the original dense model.

Static KV-Cache. MoA only maintains the tokens within the span of each head, thereby preventing growth in the KV-Cache size. This strategy eliminates the need for additional memory allocation.

Reduced Attention Computation. MoA with features reduced density in attention span and KV-Cache. It decreases the computation and memory access required for attention computation.

Table 9: Efficiency analysis of different frameworks on 7B and 13B models. H2O and MoA use 50% density. GPU memory evaluated with batch sizes 8 (7B model) and 4 (13B model).

Size	Framework	Memory (GB)		
		4k	8k	16k
7B	FlashAttn2	28.5	44.4	76.3
	H2O	36.9	OOM	OOM
	MoA	22.7	32.9	53.5
13B	FlashAttn2	36.8	49.2	74.0
	H2O	40.4	77.9	OOM
	MoA	32.0	39.6	55.0

Table 10: Compression overhead for various stages of MoA across models with differing parameter sizes, reported as the amount of GPU \times latency, except when only one GPU is used. Larger models necessitate more GPUs due to model parallelism. All stages utilize GPUs, except for the Optimize stage, which uses the CPU.

Stage	7B LLM	13B LLM	70B LLM
Calibration Data Gen.	10min	15min	$2 \times 60\text{min}$
Profile	20min	$2 \times 25\text{min}$	$8 \times 210\text{min}$
Optimize (CPU)	30min	25min	100min
Validate	35min	40min	$2 \times 140\text{min}$
Total Latency	1h 35min	1h 45min	8h 30min
Total GPU Time	1h 5min	1h 45min	34h 40min

Table 11: Progressive compression overhead for various stages of MoA with respect to different parameter sizes and calibration (validation) dataset sizes.

Stage	Complexity w.r.t parameter size	Complexity w.r.t dataset size
Calibration Dataset Gen.	Linear	Linear
Profile	Linear	Linear
Optimize	Polynomial \sim Exponential for #Head	Irrelevant
Validate	Linear	Linear
Empirical Latency	Almost Linear	Linear

Increased Batch Size. With the reduced size of KV-Cache, MoA supports a larger batch size, contributing to the increase in throughput.

B.2.2 AUTOMATIC COMPRESSION PIPELINE OVERHEAD

We present a detailed breakdown of the time usage of MoA pipeline. Table 10 summarizes the time required for various crucial phases within the MoA framework, encompassing calibration dataset generation, profiling, optimization, and validation, on the Vicuna-13B model.

Profiling is the most resource-demanding part of our pipeline. For a 13b model with an 8k profile length, two A100 GPUs are required. In other cases, we only need one single GPU. Profiling on a 13b model with an 8k profile length and 50 data items takes 15 minutes. Profiling on 4k and 2k lengths takes less than 5 minutes each.

On the Intel(R) Xeon(R) Platinum 8358 2.60 GHz CPU, the optimization concludes within approximately 25 minutes. Typically, this phase generates around 10 compression plans. Validating each one of the compression plans takes about 4 minutes, totaling around 40 minutes.

We also show the progressive compression overhead for MoA in Table 11.

B.3 ABLATION STUDY

B.3.1 CALIBRATION DATASET

In this section, we validate the robustness of our calibration dataset design principles. We select three sub-tasks and respective datasets from the LongBench benchmark, including Qasper (Dasigi et al., 2021), MultiNews (Fabbri et al., 2019), and TREC (Li & Roth, 2002; Hovy et al., 2001). We use their training set to construct the calibration dataset, and use their respective test set in LongBench to calculate the score. Following Section 5, all calibration datasets are constructed using the original model’s response to the context and questions as the supervision.

As shown in Table 12, we find that as long as the calibration dataset conforms to the long-range dependency and model alignment highlighted in section 5, the specific choice of the dataset is less important. Calibration datasets with long dependency and model alignment show somewhat similar

Table 12: Performance comparison on various test sets, using different calibration sets. Tested on Vicuna-7B model. The result is tested with 50% density MoA on LongBench (Bai et al., 2023) 0-4k split.

Dataset	Long Dep. & Align Model	Qasper	Test Score MultiNews	TREC	Avg. Score
Original	NA	28.6	28.2	56.0	37.6
RedPajama	✗	20.6 (-8.0)	19.6 (-8.6)	66.0 (+10.0)	35.4 (-2.2)
Qasper	✓	25.6 (-3.0)	27.8 (-0.4)	55.0 (-1.0)	36.1 (-1.5)
MultiNews	✓	29.0 (+0.4)	27.5 (-0.7)	54.0 (-2.0)	36.8 (-0.8)
TREC	✓	27.3 (-1.3)	27.3 (-0.9)	55.0 (-1.0)	36.5 (-1.1)

test results on various datasets. Additionally, they all show strong generalization power to test sets other than their respective calibration dataset.

In contrast, the RedPajama dataset without long-range dependency and model alignment shows large variance on various test sets. It also differs from the performance of the original dense model, which may incur unexpected behaviors after compression. Note that though all datasets exhibit long dependency, the questions in the TREC dataset can be answered without long context. The context in the TREC dataset of LongBench is the many-shot examples, each showing a short sentence and its classification result, while the question is to classify a new short sentence. Although the context helps to determine the complete set of 50 classes, the model can also directly clarify the sentence without any context based on common knowledge. It may contribute to a high score on the TREC test set with the RedPajama calibration dataset.

C COMPRESSION PLAN ANALYSIS

C.1 STATISTICS ON RULES DISCOVERED BY MOA

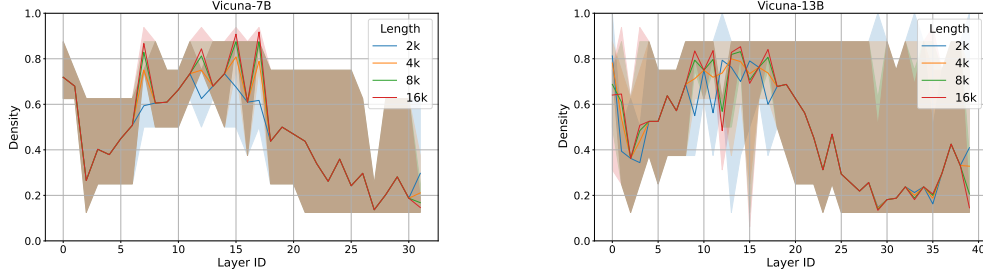


Figure 10: The MoA mask density across layers for different LLMs.

This subsection provides empirical evidence for rules discovered by MoA as mentioned in Section 6.5. The lines and spans in Figure 10 show that all heads at the first few layers generally need a high KV-Cache density. Following that, a few layers generally only require medium density. Then, in the final layers, most heads require low density, while some outlier heads need high density. This observation conforms to previous findings of the intrinsic dimension of LLM Valeriani et al. (2023). The geometry of density is similar to the intrinsic dimension of LLM, with two local minima. As observed in Figure 10, layers with lower average density (smaller values on the lines) typically display a wider range of density (wider shades). Figure 11 validates such observation. This observation confirms the need for heterogeneous attention rules within the same layer.

C.2 CONNECTIONS BETWEEN MOA RULE AND SEMANTIC

In this section, we invest the masks acquired with MoA and show the interpretable semantics of the masks. Previous works manually restrict the attention pattern of the model, which may harm

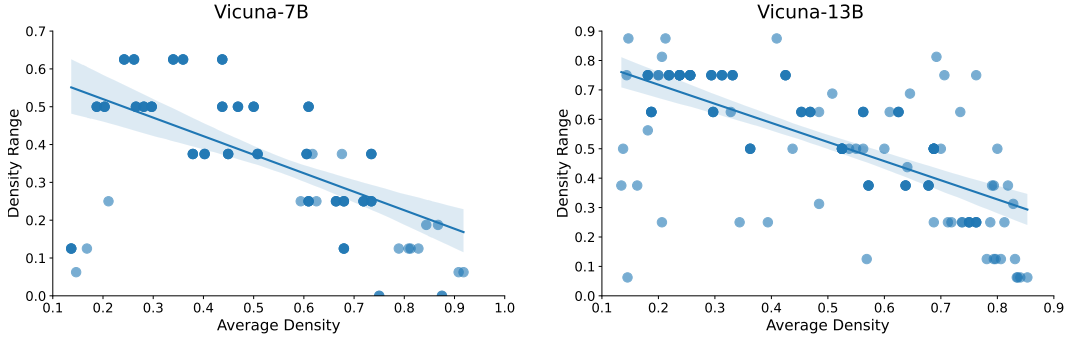


Figure 11: The MoA mask’s average density and the density range for each layer for different LLMs.

the semantics learned by the dense model. In contrast, MoA preserves the semantics with statistic analysis and optimization. We use visualization, human interpretation and quantitative methods to analyze the semantics of the original model and to verify whether MoA captures such semantics.

C.2.1 MASK VISUALIZATION AND SEMANTIC CATEGORIZATION

Given any token, two kinds of information are used as the model inputs: position encoding and token embedding. Position encoding indicates the absolute (Zhang et al., 2022) or relative positions (Touvron et al., 2023) of tokens in the sentence. Token embedding maps different tokens as different vectors. The attention head h responds to both information and output the corresponding attention value A_h . As shown in equation 6, we denote the influence of position and token of head h as function P_h and T_h , respectively. The attention value $A_{h,i,j}$ between the i th and j th token t_i and t_j is determined by the combination f_h of position and token influence functions.

$$A_{h,i,j} = \mathbb{A}_h(t_i, t_j, i, j) = f_h(P_h(i, j), T_h(t_i, t_j)) \quad (6)$$

Figure 2 visualizes two typical heads that are either dominated by position P or token T function. For the first attention head in Figure 2, the local positional attention is clearly observed. In this head, whatever sentences are given, each token pays major attention to the first token and the prior token. As a result, the mean attention matrix accumulates extremely large attention values at the first column and the sub-diagonal. In contrast, the second attention head in Figure 2 lays more emphasis on content-based attention. Since the position distribution of important tokens are generally random, the attention matrix can show large attention values at any position. It results in a mean attention matrix without extreme mean attention values.

In conclusion, the mean attention matrix of different sentences provides a valuable insight of whether attention values of an attention head is more position-based or content-based. Intuitively, the more uneven the attention matrix value distribution is, the more position-based the head is.

C.2.2 QUANTITATIVE SEMANTIC ANALYSIS

We quantify how much the attention head is position-based and analyze whether MoA successfully utilizes such semantics through the evaluate-generate-optimization pipeline. We model equation 6 with a linear approximation. P_h and T_h are random variables with the same expectation μ and standard variance δ for all heads. For attention head h , the weight factor α_h evaluates the relatively influence of position and token to the final attention value.

$$A_{h,i,j} = \alpha_h P_h(i, j) + (1 - \alpha_h) T_h(t_i, t_j) \quad (7)$$

Given the randomness of token positions in long context, we assume that the token position and its content are irrelevant. For different sentences s , the expectation \mathbb{E}_t of the attention value between position i and j can be expressed as follows. Note that it excludes the matrix diagonal since $T_h(t_i, t_j), i \neq j$ and $T_h(t_i, t_i)$ may follow different distributions.

$$\begin{aligned}
\mathbb{E}_t[A_{h,i,j}] &= \frac{1}{S} \sum_{s=1}^S \left(\alpha_h P_h(i,j) + (1 - \alpha_h) T_h(t_i^{(s)}, t_j^{(s)}) \right) \\
&= \alpha_h P_h(i,j) + (1 - \alpha_h) \frac{1}{S} \sum_{s=1}^S T_h(t_i^{(s)}, t_j^{(s)}) \\
&= \alpha_h P_h(i,j) + (1 - \alpha_h) \mu_T, \forall i > j
\end{aligned} \tag{8}$$

The standard division σ_p of \mathbb{E}_t over different positions of the attention matrix is

$$\begin{aligned}
\sigma_p(\mathbb{E}_t[A_{h,i,j}]) &= \sqrt{\frac{2}{(1+N)N} \sum_{i,j \in [1,N], i > j} [(\alpha_h P_h(i,j) + (1 - \alpha_h) \mu_T) - (\alpha_h \mu_P + (1 - \alpha_h) \mu_T)]^2} \\
&= \alpha_h \delta_p
\end{aligned} \tag{9}$$

We name $\sigma_p(\mathbb{E}_t[A_{h,i,j}])$ the Standard division of Expectation (SoE) of head h . Note that the expectation is taken over different sentences, while the standard division is taken over different attention positions. Since δ_p is the same for all heads, we derive that the position impact α_h is proportional to the SoE of different heads.

The conclusion quantifies the observation stated in Section C.2.1. Intuitively, SoE shows how uneven the mean attention matrix is, thus showing the influence of position to the attention values. MoA’s generated mask density shows positive relation with SoE, suggesting that MoA successfully captures the semantic information of the dense language model as shown in Figure 12.

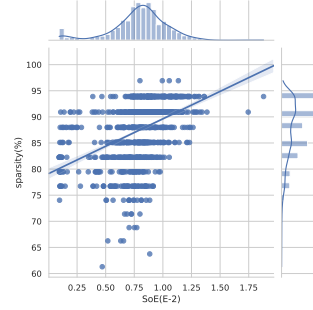


Figure 12: Positive correlation between MoA’s mask sparsity and head’s dependency on position (SoE).

D AUTOMATIC PIPELINE DETAILS

D.1 ADDITIONAL ORACLE ON ELASTIC PATTERN DESIGN

We visualize the attention matrix of the same attention heads across three additional tasks in Figure 13, as an extension of Figure 2. The consistent attention span across tasks sheds light on the strong cross-dataset generalization ability of our MoA method.

D.2 DERIVATION OF ATTENTION INFLUENCE

We use the first-order Taylor expansion to calculate the influence of each attention value. This approximation approach is supported by methodologies commonly employed in other LLM compression approaches (Li et al., 2024a; Shi et al., 2021; Das et al., 2023; Jiang et al., 2023).

As discussed in Section 4.1, when masking out attention value $A_{h,i,j}$ at head h , row i , and column j , it also influences the attention values in the same row by $\Delta A_{h,i,n|j}$.

$$\begin{aligned}
A_{h,i,n} &= \frac{e^{S_{h,i,n}}}{\sum_j e^{S_{h,i,j}}} \\
\Delta A_{h,i,n|j} &= \begin{cases} -A_{h,i,n}, & n = j \\ A_{h,i,n} (\sum_j e^{S_{h,i,j}} / \sum_{j \neq n} e^{S_{h,i,j}} - 1), & n \neq j \end{cases}
\end{aligned} \tag{10}$$

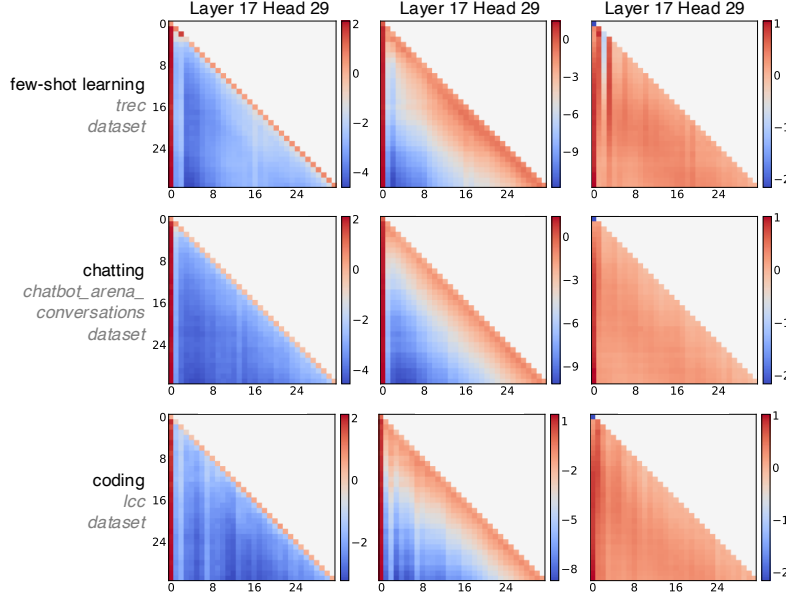


Figure 13: Examples of attention matrices from different attention heads (columns) and tasks (rows) of the Vicuna-7B model. The attention matrices were averaged over 256 data items per dataset. The same head shows a similar attention span across different tasks, explaining the robust cross-dataset generalizability of our method.

Following the definition, the attention influence \mathbf{E}_h is calculated as follows:

$$E_{h,i,j} = \sum_n \frac{\partial L}{\partial A_{h,i,n}} \cdot \Delta A_{h,i,n|j} \quad (11)$$

Given Equation 11 and 10, we derive Equation 3 as follows. For notation simplicity, we omit the head index h here.

$$\begin{aligned}
E_{i,j} &= \sum_n \frac{\partial L}{\partial A_{i,n}} \cdot \Delta A_{i,n|j} \\
&= \frac{\partial L}{\partial A_{i,j}} \cdot (-A_{i,j}) + \sum_{n \neq j} \frac{\partial L}{\partial A_{i,n}} \cdot A_{i,n} \cdot \left(\frac{\sum_k e^{S_{i,k}}}{\sum_{k \neq j} e^{S_{i,k}}} - 1 \right) \\
&= \frac{\partial L}{\partial A_{i,j}} \cdot (-A_{i,j}) + \sum_{n \neq j} \frac{\partial L}{\partial A_{i,n}} \cdot A_{i,n} \cdot \frac{e^{S_{i,j}}}{\sum_k e^{S_{i,k}} - e^{S_{i,j}}} \\
&= \frac{\partial L}{\partial A_{i,j}} \cdot (-A_{i,j}) + \sum_{n \neq j} \frac{\partial L}{\partial A_{i,n}} \cdot A_{i,n} \cdot \frac{e^{S_{i,j}} / \sum_k e^{S_{i,k}}}{1 - e^{S_{i,j}} / \sum_k e^{S_{i,k}}} \\
&= \frac{\partial L}{\partial A_{i,j}} \cdot (-A_{i,j}) + \sum_{n \neq j} \frac{\partial L}{\partial A_{i,n}} \cdot A_{i,n} \cdot \frac{A_{i,j}}{1 - A_{i,j}} \\
&= \frac{\partial L}{\partial A_{i,j}} \cdot (-A_{i,j}) - \frac{\partial L}{\partial A_{i,j}} \cdot A_{i,j} \cdot \frac{A_{i,j}}{1 - A_{i,j}} + \sum_n \frac{\partial L}{\partial A_{i,n}} \cdot A_{i,n} \cdot \frac{A_{i,j}}{1 - A_{i,j}} \\
&= \frac{\partial L}{\partial A_{i,j}} \cdot \left(-\frac{A_{i,j}}{1 - A_{i,j}} \right) + \frac{A_{i,j}}{1 - A_{i,j}} \cdot \sum_n \frac{\partial L}{\partial A_{i,n}} \cdot A_{i,n} \\
&= -\frac{A_{i,j}}{1 - A_{i,j}} \left(\frac{\partial L}{\partial A_{i,j}} - \sum_n \frac{\partial L}{\partial A_{i,n}} \cdot A_{i,n} \right)
\end{aligned} \quad (12)$$

It is worth noting to mention that it can also be formulated as matrix multiplications:

$$\mathbf{E}_h = \frac{\mathbf{A}_h}{1 - \mathbf{A}_h} \cdot \left(\frac{\partial L}{\partial \mathbf{A}_h} - \left(\frac{\partial L}{\partial \mathbf{A}_h} \cdot \mathbf{A}_h \right) \mathbb{1}^{N \times N} \right). \quad (13)$$

D.3 OPTIMIZATION DETAILS

D.3.1 OPTIMIZING AT SINGLE LENGTH

The optimization problem is formulated as follows:

$$\arg \min \Delta L = \sum_h \Delta L_{h,r_h}, \quad \text{s. t.} \quad \frac{1}{H} \sum_h d_{r_h} \leq d_{\text{constr}}. \quad (14)$$

To transform the optimization problem into a standard Mixed-Integer Programming (MIP) framework, we introduce the binary variable $X_{h,r_h} \in \{0, 1\}$. It indicates whether to select rule r_h for the attention head h . Assume the model has H attention head, and head h has R_h elastic rules.

$$\arg \min \frac{1}{H} \sum_{h=0}^{H-1} \sum_{r_h=0}^{R_h-1} \Delta L_{h,r_h} X_{h,r_h} \quad \text{s. t.} \quad (15a)$$

$$\sum_{r_h=0}^{R_h-1} X_{h,r_h} = 1, \quad h \in \{0, \dots, H-1\} \quad (15b)$$

$$\frac{1}{H} \sum_{h=0}^{H-1} \sum_{r_h=0}^{R_h-1} d_{r_h} X_{h,r_h} \leq d_{\text{constr}} \quad (15c)$$

$$0 \leq X_{h,r_h} \leq 1, X_{h,r_h} \in \mathbb{Z}, \quad \forall h \in \{0, \dots, H-1\}, \forall r_h \in \mathbb{R} \quad (15d)$$

In this formulation, (15a) serves as the objective function to minimize the loss, subject to the constraints that each matrix selects exactly one compression plan (15b), and the average density does not exceed d_{constr} (15c). Finally, (15d) enforces that X_{h,r_h} is a binary variable, indicating the selection of plans.

Additionally, to enforce the restriction that each model layer only has a limited number of different plans, we bound the norm of element-wise multiplication of $\mathbf{X}_h = [X_{h,0} \quad X_{h,1} \quad \dots \quad X_{h,R_h-1}]^\top$ in a single layer.

D.3.2 OPTIMIZING AT MULTIPLE LENGTHS

With the ability to optimize at a single length, we utilize the same framework for multi-objective MIP across various lengths. The key is to transform the multi-objective MIP problem into several single-objective MIP problems (Paria et al., 2018). We utilize the idea of epsilon-constraint method (Yv et al., 1971).

We first select each input length as our primary objective to perform the single-objective optimization on it while simultaneously recording the outcomes of other objectives. Specifically, for N distinct objectives, we do single-objective MIP optimization on the i -th objective, getting minimum loss $\Delta L_i^{(N_i)}$, and we concurrently collect losses of other objectives $\Delta L_i^{(N_j)}$ for $j \neq i$. This process allows us to establish the range of loss $R^{(N_j)} = [\min_i \Delta L_i^{(N_j)}, \max_i \Delta L_i^{(N_j)}]$ for each objective. Then, we iterate through each objective again. Compared with the original multi-objective optimization in Equation 5, we now consider other objectives as constraints. To implement this, we partition each loss range $R^{(N_j)}$ of other objectives $j \neq i$ into M uniform intervals $S_k^{(N_j)}$, where $0 \leq k < M$. We then solve the MIP problems for each objective i and iterating through the constraint intervals:

$$\arg \min_{r_h \in \mathbb{R}} \Delta L^{(N_i)} \quad \text{s. t.} \quad \frac{1}{H} \sum_{h=1}^H d_{r_h}^{(N_i)} \leq d_{\text{constr}}^{(N_i)}, \forall N_i \in \mathbb{N}_{\text{constr}}; \quad \Delta L^{(N_j)} \in S_{k_j}^{(N_j)}, \forall j \neq i. \quad (16)$$

where this optimization is performed for each i ranging from 0 to N . For each j , k_j can vary independently from 0 to M . For efficiency consideration, we set the number of intervals as five. Finally, the results that do not conform to the Pareto front requirements are removed, resulting in the final Pareto front set of our multi-objective optimization problem.